Phase transitions and flux-loop metastable states in rotating turbulence

P. Clark Di Leoni[1], A. Alexakis[2], L. Biferale[3] and M. Buzzicotti[3]

[1]*Department of Mechanical Engineering, Johns Hopkins University, Baltimore, Maryland 21218, USA.*
[2]*Laboratoire de Physique de l'École Normale Supérieure,*
CNRS, PSL Research University, Sorbonne Université,
Université de Paris, F-75005 Paris, France. and
[3]*Dept. Physics and INFN, University of Rome "Tor Vergata", Italy.*
(Dated: February 21, 2020)

By using direct numerical simulations of up to a record resolution of 512x512x32768 grid points we discover the existence of a new metastable out-of-equilibrium state in rotating turbulence. We scan the phase space by varying both the rotation rate (proportional to the inverse of the Rossby number, Ro) and the dimensionless aspect ratio, $\lambda = H/L$, where L and H are the sizes of the domain perpendicular and parallel to the direction of rotation, respectively. We show the existence of three turbulent phases. For small Ro but finite λ, we have a split cascade where the injected energy is transferred to both large and small scales. For large λ and finite Ro there is no inverse cascade and the energy is transferred forward in Fourier space only. Surprisingly, between these two regimes, a third phase is observed as reported here for the first time. Consequently, for certain intervals of Ro and λ, energy is no longer accumulated at arbitrarily large scales, rather it stops at some characteristic intermediate length-scales from where it is then redistributed forward in Fourier space, leading to a flux-loop mechanism where the flow is out of equilibrium with vanishing net flux, and non-vanishing heterochiral and homochiral sub-fluxes. The system is further characterized by the presence of metastability and critical slowing down, explaining why previous experiments and numerical simulations were not able to detect this phenomenon, requiring extremely long observation time and huge computational resources.

INTRODUCTION. Statistical systems can develop critical behaviour, where abrupt macroscopic changes happen when varying some control parameter, like temperature or magnetic field [1]. Averaged quantities can show discontinuous or continuous variations across the critical lines/points in the phase space where the transition occurs. In many cases, experimental and numerical realizations are affected by long transients that are generated due to the presence of metastable states corresponding to local minima of the (free) energy. There have been many attempts to transfer such descriptions to out-of-equilibrium systems quantitatively [2, 3]. The critical behaviour of stationary systems in the presence of energy injection mechanisms, dissipation and non-vanishing fluxes remains a major topic of current research in fluid-dynamics, granular and active matter and lacks systematic theoretical understanding [4–6]. A paradigmatic example of (phase) transition is the sudden jump from laminar to turbulent dynamics that is observed in Poiseuille and Couette flows when changing the forcing intensity [7–9]. In this paper, we investigate the important case of rotating turbulence where the control parameter, given by the intensity of the Coriolis force, affects the symmetries of the macroscopic flow but not the energy injection rate [10–14]. In this set-up, it is known that for sufficiently weak rotation rate, Ω, the system behaves as 3D homogeneous and isotropic turbulence transferring energy to small scales only (*forward energy cascade*), while for Ω above a critical value, Ω_c, 3D fluctuations are sufficiently suppressed, the flow becomes quasi-two dimensional and energy is transferred with a *split cascade* to large scales also [5, 15]. As as the domain size H in the direction of rotation becomes larger, Ω_c increases [16–18]. Arguments based on wave-turbulence theory suggest that the inverse flux vanishes in the infinite volume limit, predicting that $\lim_{H\to\infty} \Omega_c \to \infty$ [19]. More recently, considering an asymptotic form of the governing equations for large Ω, it was shown that $\Omega_c \propto H$ [20]. However, for finite Ω we do not know the precise functional dependence of the boundary $\Omega_c(H)$ nor the nature of the transition. Despite of the importance of such questions for geophysical and engineering applications we still do not have a satisfying understanding of any of them. While trying to address these problems, we discovered that the physics is even richer due to the existence of a new region in the (λ, Ro) phase-space, where turbulence develops a third, non-trivial, macroscopic out-of-equilibrium state, characterized by a *flux-loop cascade*, where the flow organises to spontaneously contain the tendency to condensate energy in larger and larger scales, entering a stationary regime and producing a quasi-ordered array of turbulent columnar vortices, akin to a vortex crystal [21]. The aim of this letter is to report about this new state of turbulent rotating flows, characterizing its peculiar statistical and dynamical properties, including metastability and critical slowing down as well as commenting about its potential importance for other turbulent realizations.

SETUP. We begin by considering the flow in a rectangular periodic domain with aspect ratio $\lambda \equiv H/L$ and dimensions $2\pi L \times 2\pi L \times 2\pi H$ in a rotating reference frame where the rotation is along the direction with dimension
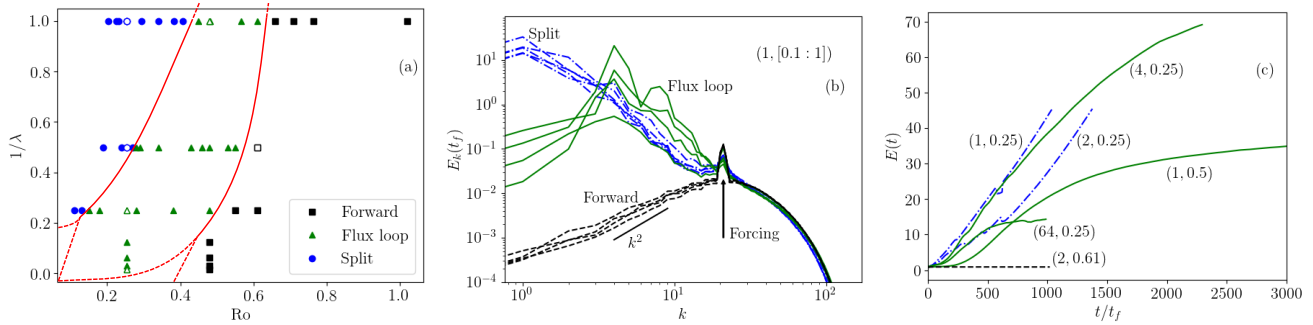
FIG. 1. (a): (λ, Ro) Phase space. Different symbols represent the three macroscopic turbulent cascade phases: forward, flux-loop and split. Red continuos line are a guide to the eye to distinguish the three phases. Red dotted-lines represents possible asymptotics behaviour in the limit $Ro \to 0$ and $\lambda \to \infty$ (see discussion in the text). (b): Instantaneous energy spectra for fixed aspect ratio, $\lambda = 1$ at different Rossby numbers $0.1 \leq Ro \leq 1$. For flux-loop and direct cascade cases the spectra are plotted in the stationary regime, for the split-cascade regime we used the final time when we stopped the simulation. (c): time evolution of the total energy, $E(t)$, for some characteristic (λ, Ro) values (represented with empty symbols in panel (a)). Line colours distinguish the three phases following the same color code of symbols in panel (a).

$2\pi H$. The governing equations for the incompressible velocity field, $\mathbf{u}$, can be written as

$$\partial_t \mathbf{u} + \mathbf{u} \cdot \nabla \mathbf{u} + 2\mathbf{\Omega} \times \mathbf{u} = -\nabla P + \nu \Delta \mathbf{u} + \mathbf{f} \quad (1)$$

where ν is the kinematic viscosity, $\mathbf{f}$ is an external forcing and $2\mathbf{\Omega} \times \mathbf{u}$ is the Coriolis force produced by the frame rotating with intensity Ω. We choose the forcing $\mathbf{f}$ to be Gaussian and delta-correlated in time, acting on a spherical Fourier shell with $|\mathbf{k}| \in [k_f, k_f + 2]$ and with amplitude $f_0 = f_1/\lambda$, so that the total injection rate $\epsilon = \langle \mathbf{f} \cdot \mathbf{u} \rangle$ remains fixed, where $\langle \bullet \rangle$ means an average over the forcing realization or on the whole fluid volume. In order to reduce viscous effects, most of the results shown have been obtained by adopting a modified hyperviscosity (see later and SM for details). In the present work, we keep $k_f L = 20$ fixed, using λ as control parameter. Besides λ the other two non-dimensional quantities are given by Reynolds, $Re = \epsilon^{1/3} k_f^{-4/3} \nu^{-1}$ and Rossby, $Ro = \epsilon^{1/3} k_f^{2/3} \Omega^{-1}$, numbers. The equations are solved using a parallel pseudo spectral code (see details in [22]) using grids as big as $512 \times 512 \times 32768$ for the largest aspect ratio $\lambda = 64$. It is important to stress that accessing high aspect ratios is key to attack the *infinite volume* limit in the direction parallel to rotation and to assess potential singular effects induced by a finite separation of the 2D plane at $k_\parallel = 0$ from the 3D modes with $k_\parallel > 0$ in Fourier space [23]. We also fixed $L = 1$ and $\epsilon = 1$.

RESULTS. Figure 1(a) summarizes the main results of our paper, showing the existence of three different macroscopic *phases* of the rotating flow in the (λ, Ro) space, consisting in (i) a pure forward cascade, (ii) a new flux-loop regime (the choice of name will become obvious later) and (iii) a split cascade regime. In Fig. 1b we show for the sub-set of simulations with $\lambda = 1$ and

at various Ro the isotropic energy spectra, defined as

$$E_k(t) = \frac{1}{2} \sum_{k \leq |\mathbf{k}| < k+1} |\hat{\mathbf{u}}_{\mathbf{k}}(t)|^2$$

where $\hat{\mathbf{u}}_{\mathbf{k}}(t)$ are the Fourier coefficients of the velocity field. The direct cascade regime (black dashed lines) does not develop any large scale fluctuations and peaks at the forcing scale. The split cascade regime (blue dash-dotted curves) showcases both forward and inverse cascades and the simulations are stopped when the peak at the largest horizontal scale, $k \simeq 1$, is well developed. The novelty here is given by the flux-loop phase (solid green lines) showing an intermediate spectral behavior. In this case, the energy spectra are much more irregular, break self-similarity and have their largest peak at an intermediate wavenumber, $k \simeq 5$. Figure 1(c) shows the evolution of the total energy, $E(t) = \sum_k E_k(t)$, for some of the most characteristic (λ, Ro) values. As expected, in the case with a forward cascade we have a constant (small) total kinetic energy as all energy input is dissipated at high wavenumbers by the viscosity. In the two data-sets showing a split cascade regime, the energy increases constantly as it is transferred to large scales without important dissipative effects. In the three flux-loop data-sets, the total energy saturates for very long times, indicating that the flux to the large scales is halted.

In Figs. 2(a)-(c) we show visualisations of the vorticity projection in the direction of the rotation axis for three characteristic data-sets representing the three different phases at late times, and in the SM we show movies comparing their time evolutions. In the split cascade regime (a), the system forms many co-rotating columnar vortices which eventually merge into one. In the forward cascade regime (c), no large scale coherent vortical structures are formed, as expected. In the new flux-loop regime (b), the columnar vortices form, but do
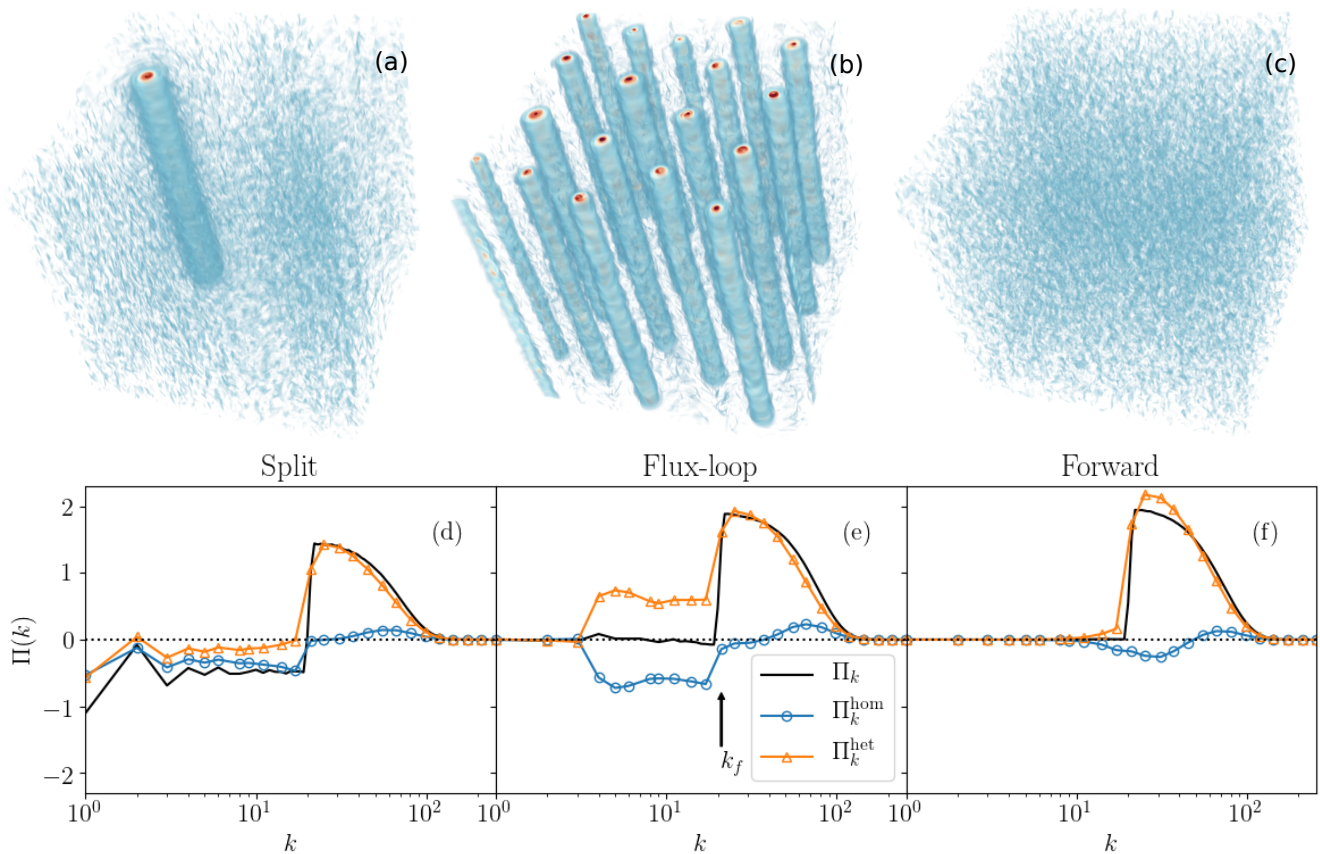
FIG. 2. (a)-(c): Visualizations of the parallel component of the vorticity for a split cascade case, a flux loop case, and a forward cascade case, respectively. (d)-(f): Total and chirally decomposed fluxes, for the three regimes shown in the top row.

not merge and get quasi stuck in a lattice-like structure that persists in time. Similar structures, deemed "vortex crystals", have been observed in systems like 2D point vortices [24, 25], 2D turbulence [26–28], Bose-Einstein condensates [29, 30], and even Jupiter's atmosphere [31]. In particular, asymmetric states where the system resembles a crystal with defects, like what is shown in Fig. 2b, have been shown to be equilibria of co-rotating point vortex systems [24, 25]. Note that in 2D randomly forced turbulence there is a symmetry between positive and negative vorticity. As a result, the kind of structures that we observe here are connected to the asymmetry between co-rotating and counter rotating vortices introduced by rotation and 3D effects.

It is worth noting that the vortex crystal state is formed in the absence of any large scale damping term to suppress the inverse cascade. The stationarity of the energy spectrum then implies that the total inverse energy flux at $k < k_f$ has to be zero. Nonetheless, the spectrum is far from the $E_k \propto k^2$ shape predicted by a simple equilibrium distribution [32, 33]. To resolve this puzzle we show in Figs. 2(d)-(f) the total energy flux, $\Pi_k = -i \sum_{|\boldsymbol{k}| \leq k} \sum_{\boldsymbol{p}+\boldsymbol{q}=\boldsymbol{k}} (\hat{\boldsymbol{u}}_{-\boldsymbol{k}} \cdot \hat{\boldsymbol{u}}_{\boldsymbol{p}})(\boldsymbol{k} \cdot \hat{\boldsymbol{u}}_{\boldsymbol{q}})$, and its exact decomposition in homochiral and heterochiral

sub-components, $\Pi_k = \Pi_k^{hom} + \Pi_k^{het}$, built in terms of Fourier triads including modes with the same or opposite helicity signatures (see SM and [23, 34] for a discussion about the importance of hetero- and homo-chiral properties for the energy cascade direction). In order to reduce fluctuations, fluxes are averaged on stationary or quasi-stationary time windows. As one can see, the forward cascade (panel f) does not show any exotic behaviour, both the total flux and it sub-components are zero in the $k < k_f$ range [35, 36]. For the split cascade phase in the range $k < k_f$ (panel d) we have the usual negative total flux as a result of the negative contributions from the two helical sub-components (in a quasi 2D regime helicity does not play any role and homo- and hetero-chiral channels are expected to be identical [37, 38]). The interesting -and non trivial- result is shown in panel (e) where the total flux for $k < k_f$ is zero, as it must be if the statistics are stationary, but it is the result of a balance between the forward, $\Pi_k^{het} > 0$, and the inverse, $\Pi_k^{hom} < 0$ sub-fluxes contributions. Hence the name of a flux-loop state [5]. This highly intricate flux-loop balance is an out-of-equilibrium effect and has already been observed in two-dimensional but three-component flows [39] and in rotating flows with only three-component mo-
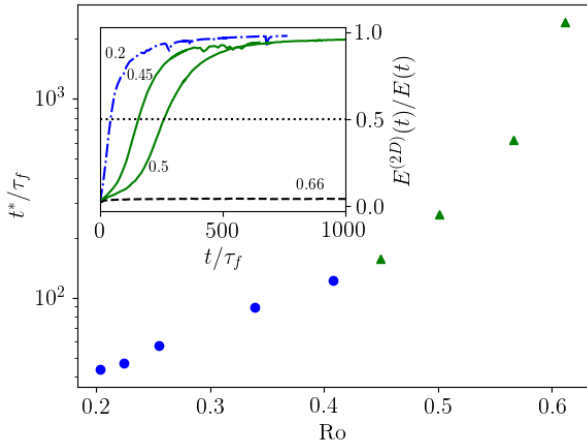
FIG. 3. Time to bidimensionalization t^* as a function of Rossby number for aspect ratio $\lambda = 1$. Inset: Ratio of the energy in the 2D modes a function of time.

tions [40] where similar peaked spectra were found.

From previous figures it is clear that the inverse cascade and the flux-loop phase are the results of a competition between a tendency to become 2D-like contrasted by some residual 3D structures that push energy forward. It is therefore interesting to assess the dynamical effects of these contrasting forces. To do that, we measured the typical time it take the energy to become concentrated on the $k_\parallel \approx 0$ 2D plane, defined as the instant of time, t^*, when the ratio $E^{(2D)}(t^*)/E(t^*)$ hits 0.5, where $E^{(2D)}(t) = \sum_{|\mathbf{k}\cdot\mathbf{\Omega}|<1} \frac{1}{2}|\hat{\mathbf{u}}_{\mathbf{k}}|^2$ is the total energy in the Fourier plane perpendicular to the rotation direction. In the inset of Fig. 3 we show the evolution of $E^{(2D)}(t)/E(t)$ as a function of time for four different values of Ro. It is clear that in both the split and the flux-loop cascades, the flow approaches asymptotically a quasi-2D state, the main difference is the time it takes to reach it. The main panel of Fig. 3 shows the time t^*/τ_f vs Ro in a log-lin plot at fixed λ, where $\tau_f = (\epsilon k_f^2)^{-1/3}$ is the characteristic time associated with the forcing. It is interesting to notice that when entering the flux-loop region, t^* increases with Ro faster than exponentially, indicating the presence of a possible divergence at the critical value of $Ro_c \simeq 0.65$. The transition from the split to the forward cascade as a function of the Rossby number has been also analyzed in a recent important study [18], but with runs that evolved until $t/\tau_f = 30$ only, and thus miss the development of the flux-loop regime. In fact, the critical Rossby number reported in [18] is around the same value where we see the transition from split to flux-loop cascades, and the growth rates they report (measured by the rate of change of the vertical correlations) depend exponentially on Ro, the same way t^* does for $Ro < 0.4$.

Two important remarks are now in order. First, the transition between split and flux-loop cascades exhibits hysteresis. If one takes a stable simulation under the flux-loop regime and sufficiently decreases Ro the vortex-crystal is destabilized, the columns merge, and the system switches to a split cascade regime. Conversely, the opposite does not happen. We have checked this explicitly. Second, and even more important, the vortex crystals formed in the flux-loop regime are metastable. For example, we observed that by evolving a simulation with parameters (λ, Ro) close to the transition from flux-loop to split cascade the vortex crystal structure is destabilized after a long time and the inverse cascade starts again (see the central panel in the SM movie). Metastability is consistent with the fact that the vortex crystal is observed at the boundary between the inverse and the forward cascade and with the existence of a critical slowing down.

CONCLUSIONS. By using huge high-performance-computing resources we have studied the (λ, Ro) phase space of rotating turbulence up to record resolution of $512 \times 512 \times 32768$ grid points. We found the existence of a new metastable flux-loop regime, where the inverse energy cascade is stopped by a delicate balance between hetero- and homo-chiral triadic non-linear interactions, leading to multiple metastable vortex-crystal like states. These states are stable for very long times but can transition to the inverse cascade regime if perturbed strongly enough.

Observations of multiple large-scale, self-organised turbulent state are becoming more and more common in the turbulent literature, having been observed in bounded flows [41], in anisotropic sheared turbulence [42], in swirling flows [43] and in magnetohydrodamic flows [44]. They play a key role for both fundamental aspects, suggesting the existence of multiple attractors in the system and applied ones, leading to huge variations in the global energetic balance for tiny changes in the control parameters. The present study relates these metastable states with the boundaries of two different states (forward and split cascading) in a phase-diagram making the connection with classical phase transitions.

Some important questions remain open, connected to the asymptotic behavior of the critical lines between different phases and the robustness of the metastable states in the limit $Ro \to 0$, $\lambda \to \infty$ and $\lambda \to 0$ (see dashed red lines in the phase-space summary of Fig. 1(a)). The presence of the flux-loop condensate prevented us from extracting a precise functional behaviour in the (λ, Ro) plane for the transition from forward to split cascade. Although the asymptotic scaling $\lambda \propto Ro^{-1}$ that was suggested in [5] and found in [20] is still plausible, the present results can not confirm nor reject this hypothesis, because of the presence of the flux-loop phase. Finally, we note that metastable properties can depend on the horizontal domain size L. If L is large enough and the size of the vortex-crystal is increased the possibility of having a destabilizing local defect increases.

_____

[1] N. Goldenfeld, *Lectures on phase transitions and the renormalization group* (CRC Press, 2018).

[2] R. Zwanzig, *Nonequilibrium statistical mechanics* (Oxford University Press, 2001).

[3] L. Berthier and G. Biroli, Reviews of Modern Physics **83**, 587 (2011).

[4] M. C. Marchetti, J.-F. Joanny, S. Ramaswamy, T. B. Liverpool, J. Prost, M. Rao, and R. A. Simha, Reviews of Modern Physics **85**, 1143 (2013).

[5] A. Alexakis and L. Biferale, Physics Reports **767**, 1 (2018).

[6] I. S. Aranson and L. S. Tsimring, Reviews of modern physics **78**, 641 (2006).

[7] G. Lemoult, L. Shi, K. Avila, S. V. Jalikop, M. Avila, and B. Hof, Nature Physics **12**, 254 (2016).

[8] M. Chantry, L. S. Tuckerman, and D. Barkley, Journal of Fluid Mechanics **824** (2017).

[9] D. Moxey and D. Barkley, Proceedings of the National Academy of Sciences **107**, 8091 (2010).

[10] P. A. Davidson, *Turbulence in rotating, stratified and electrically conducting fluids* (Cambridge University Press, 2013).

[11] A. Campagne, B. Gallet, F. Moisy, and P.-P. Cortet, Physics of Fluids **26**, 125112 (2014).

[12] A. Pouquet and R. Marino, Physical review letters **111**, 234501 (2013).

[13] E. Yarom and E. Sharon, Nature Physics **10**, 510 (2014).

[14] P. Sagaut and C. Cambon, *Homogeneous turbulence dynamics*, Vol. 10 (Springer, 2008).

[15] L. M. Smith and F. Waleffe, Physics of fluids **11**, 1608 (1999).

[16] E. Deusebio, G. Boffetta, E. Lindborg, and S. Musacchio, Phys. Rev. E **90**, 023005 (2014).

[17] T. Pestana and S. Hickel, Physical Review E **99**, 053103 (2019).

[18] T. Pestana and S. Hickel, Journal of Fluid Mechanics **885** (2020), 10.1017/jfm.2019.976.

[19] S. Galtier, Physical Review E **68**, 015301 (2003).

[20] A. van Kan and A. Alexakis, arXiv preprint arXiv:1912.05394 (2019).

[21] H. Aref, P. K. Newton, M. A. Stremler, T. Tokieda, and D. L. Vainchtein, *Vortex crystals*, text (Department of Theoretical and Applied Mechanics (UIUC), 2002).

[22] L. Biferale, F. Bonaccorso, I. M. Mazzitelli, M. A. van Hinsberg, A. S. Lanotte, S. Musacchio, P. Perlekar, and F. Toschi, Physical Review X **6**, 041036 (2016).

[23] F. Waleffe, Physics of Fluids A: Fluid Dynamics **5**, 677 (1993).

[24] H. Aref and D. L. Vainchtein, Nature **392**, 769 (1998).

[25] H. Aref, P. K. Newton, M. A. Stremler, T. Tokieda, and D. L. Vainchtein, Adv. Appl. Mech. **39**, 1.

[26] K. S. Fine, A. C. Cass, W. G. Flynn, and C. F. Driscoll, Physical Review Letters **75**, 3277 (1995).

[27] X.-P. Huang and C. Driscoll, Physical review letters **72**, 2187 (1994).

[28] J. Jiménez and A. Guegan, Physics of Fluids **19**, 085103 (2007).

[29] J. Abo-Shaeer, C. Raman, J. Vogels, and W. Ketterle, Science **292**, 476 (2001).

[30] P. K. Newton and G. Chamoun, SIAM Review **51**, 501 (2009).

[31] A. Adriani, A. Mura, G. Orton, C. Hansen, F. Altieri, M. L. Moriconi, J. Rogers, G. Eichstädt, T. Momary, A. P. Ingersoll, G. Filacchione, G. Sindoni, F. Tabataba-Vakili, B. M. Dinelli, F. Fabiano, S. J. Bolton, J. E. P. Connerney, S. K. Atreya, J. I. Lunine, F. Tosi, A. Migliorini, D. Grassi, G. Piccioni, R. Noschese, A. Cicchetti, C. Plainaki, A. Olivieri, M. E. O'Neill, D. Turrini, S. Stefani, R. Sordini, and M. Amoroso, Nature **555**, 216 (2018).

[32] V. Dallas, S. Fauve, and A. Alexakis, Physical review letters **115**, 204501 (2015).

[33] A. Alexakis and M.-E. Brachet, Journal of Fluid Mechanics **872**, 594 (2019).

[34] F. Waleffe, Physics of Fluids A: Fluid Dynamics (1989-1993) **4**, 350 (1992).

[35] A. Alexakis, Journal of Fluid Mechanics **812**, 752 (2017).

[36] G. Sahoo and L. Biferale, Fluid Dynamics Research **50**, 011420 (2018).

[37] L. Biferale, M. Buzzicotti, and M. Linkmann, Physics of Fluids **29**, 111101 (2017).

[38] M. Buzzicotti, H. Aluie, L. Biferale, and M. Linkmann, Physical Review Fluids **3**, 034802 (2018).

[39] L. Biferale, M. Buzzicotti, and M. Linkmann, Physics of Fluids **29**, 111101 (2017).

[40] M. Buzzicotti, P. Clark Di Leoni, and L. Biferale, The European Physical Journal E **41**, 131 (2018).

[41] S. G. Huisman, R. C. A. v. d. Veen, C. Sun, and D. Lohse, Nature Communications **5**, 1 (2014).

[42] K. P. Iyer, F. Bonaccorso, L. Biferale, and F. Toschi, Phys. Rev. Fluids **2**, 052602 (2017).

[43] D. Faranda, Y. Sato, B. Saint-Michel, C. Wiertel, V. Padilla, B. Dubrulle, and F. Daviaud, Phys. Rev. Lett. **119**, 014502 (2017).

[44] J. V. Shebalin, Physics of Plasmas **17**, 092303 (2010).

λ	N_z	Ω	Ro	Regime	λ	N_z	Ω	Ro	Regime
1	512	37.5	0.204	Split	2	1024	22.5	0.340	Flux-loop
1	512	34	0.225	Split	2	1024	18	0.425	Flux-loop
1	512	33	0.232	Split	2	1024	16.5	0.464	Flux-loop
1	512	30	0.255	Split	2	1024	14.5	0.528	Flux-loop
1	512	26	0.294	Split	2	1024	13.9	0.551	Flux-loop
1	512	22.5	0.340	Split	2	1024	12.5	0.613	Forward
1	512	20	0.382	Split	4	2048	70	0.109	Split
1	512	18.75	0.408	Split	4	2048	60	0.128	Split
1	512	17	0.450	Flux-loop	4	2048	50	0.153	Flux-loop
1	512	15	0.510	Flux-loop	4	2048	42.5	0.180	Flux-loop
1	512	15	0.501	Flux-loop	4	2048	30	0.249	Flux-loop
1	512	13.5	0.566	Flux-loop	4	2048	27.5	0.279	Flux-loop
1	512	12.5	0.611	Flux-loop	4	2048	20	0.383	Flux-loop
1	512	11.6	0.659	Forward	4	2048	15	0.507	Flux-loop
1	512	10.8	0.708	Forward	4	2048	13.9	0.551	Forward
1	512	10	0.764	Forward	4	2048	12.5	0.613	Forward
1	512	7.5	1.019	Forward	8	4096	30	0.246	Flux-loop
2	1024	40	0.191	Split	16	8192	30	0.246	Flux-loop
2	1024	32	0.239	Split	32	16384	30	0.244	Flux-loop
2	1024	30	0.242	Split	64	32768	30	0.247	Flux-loop
2	1024	28	0.274	Split	8	4096	15	0.511	Forward
2	1024	15	0.481	Split	16	8192	15	0.480	Forward
2	1024	27.5	0.278	Flux-loop	32	16384	15	0.481	Forward
2	1024	26.4	0.290	Flux-loop	64	32768	15	0.479	Forward

TABLE I. All simulations were produced with a horizontal resolution of $N_x = N_y = 512$, box size $L = 2\pi$, hyperviscosity of order $\alpha = 2$, forcing wavenumber in the range range $[k_f, k_f + 2]$ with $k_f = 20$, forcing amplitude $f_0 = f_1/\lambda$ with $f_0 = 1.66$, viscosity $\nu = 4 \times 10^{-7}$, energy injection rate of $\epsilon = 2.02$ and Reynolds number defined on the forcing scale $Re = 125$ (see main text). The parameters shown in the table are the box aspect ratio $\lambda = H/L$, the number of collocation points in the vertical direction N_z, rotation rate Ω, Rossby number defined in terms of the energy injection properties, $Ro = (\varepsilon_f k_f^2)^{1/3}/\Omega$, and the regime the simulation is in.

SUPPLEMENTAL MATERIAL

Numerical Simulations

We performed a series of direct numerical simulations (DNS) of the incompressible Navier-Stokes equations (see Eqs. (1) in the main text) where the normal viscosity has been replaced with hyper-viscous dissipation:

$$\begin{cases} \partial_t \boldsymbol{u} + \boldsymbol{u} \cdot \nabla \boldsymbol{u} + 2\boldsymbol{\Omega} \times \boldsymbol{u} = -\nabla p + \nu(-1)^{\alpha+1}\Delta^\alpha \boldsymbol{u} + \boldsymbol{f} \\ \nabla \cdot \boldsymbol{u} = 0, \end{cases} \tag{2}$$

with $\alpha = 2$. The motivation to use hyper-viscosity comes from request to minimize viscous effects at the forcing scale at the expense of generating spectral bottlenecks at high wavenumbers [?], allowing the inverse energy cascade to develop with minimal Reynolds effects. For a few cases, we made sure to test that increasing the Reynolds numbers do not introduce important differences with what reported here. In Table I we provide a list of all parameters used in each of the simulations presented in this paper.

Helical decomposition

In this section we provide the definition of the helical-fluxes calculated in Fig.2(a-c) of the main text. For this purpose we exploit the decomposition of any incompressible 3D flow into helical modes proposed by [34?]. From the incompressibility assumption it follows that $\boldsymbol{u}(\boldsymbol{x})$ is a solenoidal vector field, hence its Fourier modes $\hat{\boldsymbol{u}}(\boldsymbol{k})$ depends only on two linearly independent degrees of freedom and we can decompose the velocity field as follows

$$\hat{\boldsymbol{u}}_{\boldsymbol{k}}(t) = \hat{\boldsymbol{u}}_{\boldsymbol{k}}^+(t) + \hat{\boldsymbol{u}}_{\boldsymbol{k}}^-(t) = \hat{u}_{\boldsymbol{k}}^+(t)\mathbf{h}_+(\boldsymbol{k}) + \hat{u}_{\boldsymbol{k}}^-(t)\mathbf{h}_-(\boldsymbol{k}) \ , \tag{3}$$

where $\mathbf{h}_\pm(\boldsymbol{k})$ are the orthogonal eigenmodes of the curl operator, hence each Fourier modes of the velocity field satisfies

$$ i\boldsymbol{k} \times \hat{\boldsymbol{u}}_{\boldsymbol{k}}^{s_{\boldsymbol{k}}} = s_{\boldsymbol{k}} \hat{\boldsymbol{u}}_{\boldsymbol{k}}^{s_{\boldsymbol{k}}} \ , \tag{4} $$

with $s_{\boldsymbol{k}} = \pm$. The homo-chiral energy fluxes is made out of triads with the same chirality:

$$ \Pi_k^{hom} = \Pi_k^{(+,+,+)} + \Pi_k^{(-,-,-)} \tag{5} $$

$$ \Pi_k^{(\pm,\pm,\pm)} = -i \sum_{|\boldsymbol{k}| \leq k} \sum_{\boldsymbol{p}+\boldsymbol{q}=\boldsymbol{k}} (\hat{\boldsymbol{u}}_{-\boldsymbol{k}}^\pm \cdot \hat{\boldsymbol{u}}_{\boldsymbol{p}}^\pm)(\boldsymbol{k} \cdot \hat{\boldsymbol{u}}_{\boldsymbol{q}}^\pm) \tag{6} $$

while the heterochiral is given by all resulting triads with two Fourier modes of opposite chirality:

$$ \Pi_k^{het} = \Pi_k - \Pi_k^{hom} \ , \tag{7} $$

where Π_k is the total energy flux defined in the main text as

$$ \Pi_k = -i \sum_{|\boldsymbol{k}| \leq k} \sum_{\boldsymbol{p}+\boldsymbol{q}=\boldsymbol{k}} (\hat{\boldsymbol{u}}_{-\boldsymbol{k}} \cdot \hat{\boldsymbol{u}}_{\boldsymbol{p}})(\boldsymbol{k} \cdot \hat{\boldsymbol{u}}_{\boldsymbol{q}}) \ . \tag{8} $$

Video material

A visualization of an inverse and a flux-loop cascade can be found in uploaded video, where we show the volume rendering of the time evolution of the vorticity component along the direction of rotation axis, $\boldsymbol{\omega}_z$, for three different simulations obtained with (Ro, λ): $(0.25, 1)$ split cascade (left panel); $(0.51, 1)$ split/flux-loop (center panel); and $(0.58, 1)$ flux-loop (right panel). Notice the metastable regime shown in the center panel where the inverse cascade first stops in to a quasi vortex crystal state and then suddenly restarts, thanks to 3D vortex merging. In the bottom row of the same video we present the energy spectra and total energy evolution for the same three simulations.